ESTIMATION OF CARBON FIBER/EPOXY INTERFACIAL NORMAL STRENGTH AND INTERFACIAL SHEAR STRENGTH BY FIBER BUNDLE TESTS

Guocheng Qi[1], Yalin Yu[2] , Boming Zhang[3] and Shanyi Du[4]

[1]School of Materials Science and Engineering, Beihang University, Beijing, China
Email: gcqi@buaa.edu.cn, web page: http://www.buaa.edu.cn
[2] Aerospace Research Institute of Materials & Processing Technology, Beijing, China
Email: yuyalin1989@126.com, web page: http://www.arimt.com
[3]School of Materials Science and Engineering, Beihang University, Beijing, China
Email: zbm@buaa.edu.cn, web page: http://www.buaa.edu.cn
[4]Center for Composite Materials and Structures, Harbin Institute of Technology, Harbin, China
Email: sydu@hit.edu.cn, web page: http://www.hit.edu.cn

Keywords: Carbon fiber reinforced composites, Fiber bundle specimen, Interfacial strength, Multiscale modelling

ABSTRACT

The fiber/matrix interface is a vital region which determines, to a great extent, the ultimate strength of the fiber reinforced composites. The assessment of interfacial strength are usually based on the mechanical test of the single filament/resin specimens, i.e., Micro-indentation, fiber pull-out, fiber fragmentation and micro-bond tests have been extensively used in the past few decades. Recently, the transverse fiber bundle tensile (TFBT) test has been successfully utilized to estimate the fiber/matrix bonding strength under different interfacial modification conditions. Higher stress concentration in the normal direction occurs at the interphase. The interfacial normal strength (INS) can be evaluated by the combination of the experimental with analytical results. Besides, the 45° fiber bundle tensile (45FBT) test was firstly proposed to bridge the assessment of interfacial shear strength and fiber bundle test approach. The interfacial shear strength (ISS) can be also calculated based on experimental results and multiscale simulation. In this work, both the TFBT test and 45FBT test were used to determine the interfacial properties of carbon fiber and epoxy. The IFS results from the 45FBT test and the INS results from the TFBT test were contrasted.

1 INTRODUCTION

It is well acknowledged that the mechanical behavior and durability of fiber reinforced polymer composites strongly depend on the fiber/matrix interface. One of the most important tasks for composite research is to develop reliable characterization approaches of the interfacial adhesion. Considering the state of interfacial stress, the interfacial normal stress in the fiber radial direction, the interfacial tangential stress in the hoop direction and interfacial shear stress in the fiber longitudinal direction should be involved in the comprehensive understanding of interfacial mechanical behavior.

Traditional approaches, for example, micro-indentation, fiber pull-out, fiber fragmentation and micro-bond tests, aim at evaluating the interfacial shear strength (ISS) based on the single filament/resin specimens. In addition, the transverse fiber bundle tensile (TFBT) test was firstly proposed by Okoroafor and Hill to assess the interfacial normal strength (INS) and has been successfully implemented to estimate the effects of interface modification on interfacial normal bonding properties. Since the obtained result of TFBT test is the apparent tensile strength which can be considered as the strength of the special fiber bundle composite structure, theoretical analysis is also necessary to explore the microscopic mechanisms and determined the interfacial strength. Furthermore, as an extension of the TFBT test, the 45° fiber bundle tensile (45FBT) test has also been developed to assess the IFSS based on the fiber bundle composite.

Compared with the single fiber interfacial test approaches, the TFBT and 45FBT tests can lead to a lower degree of scatter between the strength values. This is mainly due to the direct use of the fiber

bundle instead of the filament picked from the fiber tows containing thousands of single fibers. In the fiber bundle tests, the actual distribution of the reinforcing fibers in the matrix can also be taken into account, which results in a more realistic micro state of stress than single fiber/resin specimens.

2 EXPERIMENTAL

The originally received commercial carbon fiber bundles Toray T700S and T800H were used in the experiment. The epoxy resin was diglycidyl ether of bisphenol A (DGEBA) (WSR618, Wuxi Bluestar Chemical Company) with an epoxide equivalent weight of 185–192 g/eq. The curing agent was JEFFAMINE® D400 polyetheramine purchased from Hustman Corporation with an amine hydrogen equivalent weight of 115 g/eq.

The preparation processes of both specimens are similar except for the degree between specimen tensile direction and fiber longitudinal direction. To fabricate the fiber bundle specimens, a length of aramid fiber bundle was placed in the slit of the mold with a dog-bone shaped groove. The mixed resin was poured into the mold after degassing and the fiber bundle was impregnated in the liquid resin until the gelation occurred. The mold was subsequently put into the oven and cured in 3 steps: 75 ℃ for 2 hours, 110 ℃ for 2 hours and 150 ℃ for 2 hours. Fig.1 (a) and (b) display the cured TFBT and 45FBT specimens, respectively.

(a)

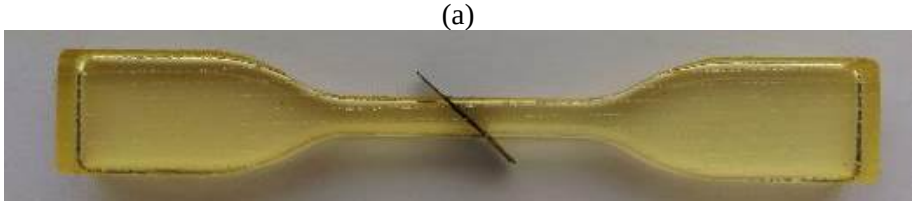

(b)

Figure 1: T700S TFBT (a) and 45FBT (b) specimens

The fiber bundle specimens should be polished to reduce the surface roughness before the tensile tests. The tensile tests were conducted on a universal machine (Instron 5565) at ambient temperature. The crosshead speed was 1mm/min. The apparent tensile strength was obtained through dividing the maximum tensile load by the area of the specimen cross section.

3 MULTISCALE MODEL

The multiscale approach is extensively used in the modeling of the behavior of heterogeneous materials. The multiscale models on the basis of the generalized methods of cells (GMC) have been established for the carbon fiber/epoxy TFBT and 45FBT approaches. Composed of macroscopic FE model and GMC micromechanics model, the multiscale model can couple the macroscopic structural scale including epoxy matrix and thin composite layer, and the microscopic scale containing fiber, matrix and interphase.

3.1 Macroscopic model

In the present analysis, the macroscopic structural level for TFBT and 45FBT samples was discretized by the commercial FE software Abaqus/Standard 6.10. As shown in Figure 2, the macro model was comprised of the homogenized fiber bundle composite layer with a thickness of 0.3 mm and the epoxy matrix. Because of the implementation of symmetry boundary conditions in OX, OY and OZ directions, only one eighth of the TFBT specimen was created. Apart from the global coordinate system (XYZ), a local coordinate system (123) was created and assigned to the composite lamina. 1, 2 and 3 represented the fiber longitudinal direction, the transverse direction and the through-

the-thickness direction respectively.

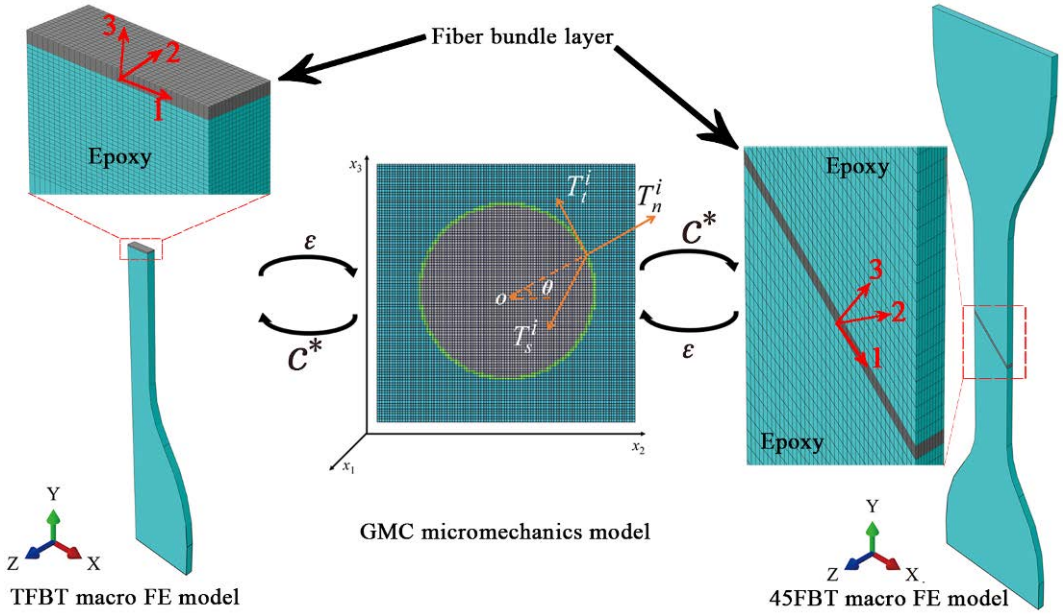

Figure 2: Multiscale model

The eight-node linear reduced solid elements (C3D8R) were employed in the FE model. Three mesh densities of 800 (20×10×4), 3200 (40×10×8) and 6400 (80×10×8) elements were compared for the composite layer. The results showed that 3200 elements were enough to give accurate local stress and strain distribution. Thus 3200 elements were utilized to mesh the fiber bundle region and 4059 (41×11×9) nodes were involved in the thin fiber bundle layer.

One parallel end of the matrix was constrained in OY direction as the boundary condition while the displacement in the OY direction was applied at the other parallel end to simulate the tensile loading. Besides, the thermal residual stress has a non-negligible influence on ultimate tensile strength of fiber bundle samples. The residual stress was mainly attributed to the mismatch of the coefficients of thermal expansion α of the carbon fiber and DGEBA/D400 resin. Thus, before the step of tensile loading, the step of thermal cooling from the glass transition temperature (50℃) to the ambient temperature (20℃) was also created to calculate the initial thermal stress of the TFBT and 45FBT specimens.

3.2 Micromechanics model

The micromechanics model based on the Generalized Method of Cells (GMC) was written in a FORTRAN code as the user-defined subroutine of the macro FE model.

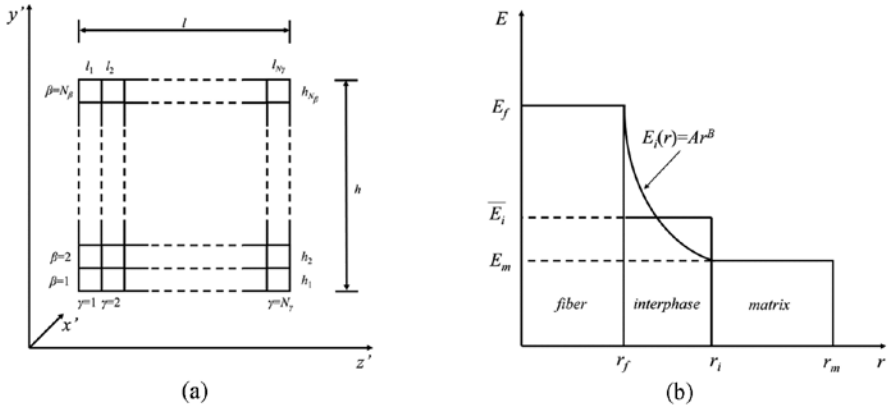

Figure 3: A typical RUC portioned into $N_\beta \times N_\gamma$ subcells in the GMC model (a) and illustration of interphase modulus (b).

As shown in, the representative unit cell was partitioned into $N_\beta \times N_\gamma$ subcells in the GMC model. Based on the assumptions of volume homogenization, traction continuity and displacement continuity, the subcell stress $\boldsymbol{\sigma}^{(\beta\gamma)} = \left\{\sigma_1^{(\beta\gamma)}, \sigma_2^{(\beta\gamma)}, \sigma_3^{(\beta\gamma)}, \sigma_{12}^{(\beta\gamma)}, \sigma_{13}^{(\beta\gamma)}, \sigma_{23}^{(\beta\gamma)}\right\}$ can be determined by the unit cell overall strain $\boldsymbol{\varepsilon} = \left\{\varepsilon_1, \varepsilon_2, \varepsilon_3, \varepsilon_{12}, \varepsilon_{13}, \varepsilon_{23}\right\}$ and the subcell compliance $\mathbf{S}^{(\beta\gamma)} = \left\{S_{11}^{(\beta\gamma)}, S_{22}^{(\beta\gamma)}, S_{33}^{(\beta\gamma)}, S_{12}^{(\beta\gamma)}, S_{13}^{(\beta\gamma)}, S_{23}^{(\beta\gamma)}\right\}$. The subcell normal stress $\left\{\boldsymbol{\sigma}_2, \boldsymbol{\sigma}_3\right\}$ can be expressed mathematically as

$$\begin{bmatrix} \mathbf{A} & \mathbf{B} \\ \mathbf{B}' & \mathbf{D} \end{bmatrix} \begin{bmatrix} \boldsymbol{\sigma}_2 \\ \boldsymbol{\sigma}_3 \end{bmatrix} = \begin{Bmatrix} \mathbf{c} \\ \mathbf{e} \end{Bmatrix} \varepsilon_1 + \begin{Bmatrix} \mathbf{H} \\ \mathbf{0} \end{Bmatrix} \varepsilon_2 + \begin{Bmatrix} \mathbf{0} \\ \mathbf{L} \end{Bmatrix} \varepsilon_3 \tag{1}$$

where $\boldsymbol{\sigma}_2 = \left[\sigma_2^{(1)}, \sigma_2^{(2)}, \cdots, \sigma_2^{(N_\gamma)}\right]$ and $\boldsymbol{\sigma}_3 = \left[\sigma_3^{(1)}, \sigma_3^{(2)}, \cdots, \sigma_3^{(N_\beta)}\right]$ contain N_γ and N_β unknown normal stresses in the individual columns and rows of the unit cell, respectively; **A**, **B**, **B'**, **D**, **c**, **e**, **H** and **L** are $N_\gamma \times N_\gamma$, $N_\gamma \times N_\beta$, $N_\beta \times N_\gamma$, $N_\beta \times N_\beta$, $N_\gamma \times 1$, $N_\beta \times 1$, $N_\gamma \times 1$ and $N_\beta \times 1$ vectors respectively, whose elements can be expressed in term of subcell dimension and compliance.

Based on the results of subcell normal stress $\sigma_2^{(\beta\gamma)}$ and $\sigma_3^{(\beta\gamma)}$, the subcell normal stress in the longitudinal direction $\sigma_1^{(\beta\gamma)}$ can be calculated as

$$\sigma_1^{(\beta\gamma)} = \frac{1}{S_{11}^{(\beta\gamma)}}\left[\varepsilon_1 - S_{12}^{(\beta\gamma)}\sigma_2^{(\beta\gamma)} - S_{13}^{(\beta\gamma)}\sigma_3^{(\beta\gamma)}\right] \tag{2}$$

The relationships between the subcell shear stress and overall shear strain are established as

$$\frac{1}{2}\left(\sum_{\beta=1}^{N_\beta} h_\beta S_{12}^{(\beta\gamma)}\right)\boldsymbol{\sigma}_{\mathbf{12}}^{(\gamma)} = h\varepsilon_{12} \tag{3}$$

$$\frac{1}{2}\left(\sum_{\gamma=1}^{N_\gamma} l_\gamma S_{13}^{(\beta\gamma)}\right)\boldsymbol{\sigma}_{\mathbf{13}}^{(\beta)} = l\varepsilon_{13} \tag{4}$$

$$\frac{1}{2}\left(\sum_{\beta=1}^{N_\beta}\sum_{\gamma=1}^{N_\gamma} h_\beta l_\gamma S_{23}^{(\beta\gamma)}\right)\boldsymbol{\sigma}_{\mathbf{23}}^{(\beta\gamma)} = hl\varepsilon_{23} \tag{5}$$

where $\boldsymbol{\sigma}_{\mathbf{12}}^{(\gamma)} = \left[\sigma_{12}^{(1)}, \sigma_{12}^{(2)}, \cdots, \sigma_{12}^{(N_\gamma)}\right]$ and $\boldsymbol{\sigma}_{\mathbf{13}}^{(\beta)} = \left[\sigma_{13}^{(1)}, \sigma_{13}^{(2)}, \cdots, \sigma_{13}^{(N_\beta)}\right]$ contain N_γ and N_β unknown normal stresses in the individual columns and rows of the unit cell, respectively. If the overall strain is determined, the subcell stress can be calculated using Equation (1)-(5). Then the subcell strain can be obtained by the subcell stress and subcell elastic properties. On the basis of the comparison results of four unit cells containing 20×20 subcells, 50×50 subcells, 100×100 subcells and 120×120 subcells respectively, the unit cell with 100×100 subcells was found accurate enough for the micromechanical analysis.

The fiber, matrix and interphase were included in the GMC model. The mechanical and thermal properties of the fiber and the matrix used in the multiscale model. The ratio of the interphase thickness to the fiber radius was assumed to be 0.04. The average interphase elastic properties were decided by power degraded laws on the basis of the fiber and matrix properties. the average interphase modulus $\overline{E_i}$ could be defined as

$$\overline{E_i} = \frac{E_f r_f}{\left(r_i - r_f\right)\left(1+B\right)}\left[\left(\frac{r_i}{r_f}\right)^{1+B} - 1\right] \tag{6}$$

where $B=\frac{\ln E_f-\ln E_m}{\ln r_f-\ln r_m}$. The interfacial moduli of T700S/epoxy, T800H/epoxy and T800S/epoxy were calculated as 9.68 GPa, 8.76 GPa and 6.96 GPa respectively. The Poisson's ratio of the interphase was assumed to be 0.37. Besides, the elastic properties of the homogeneous orthotropic composite layer were predicted using the GMC model and the thermal properties were calculated by the rule of mixture.

3.3 Multiscale failure analysis

Generally, fiber breakage under longitudinal tension or compression (no buckling) can be considered a brittle behavior. The failure of fiber follows maximum longitudinal stress failure criterion expressed as

$$\sigma_c \le \sigma_1 \le \sigma_t \tag{7}$$

in which σ_c and σ_t stand for the compressive strength and tensile strength of the fiber respectively.

The modified Tresca criterion is adopted for the matrix. The criterion can be written as

$$\tau_{\max}=S_0-\mu I_1 \ge S_m;\left(S_0=\frac{C_m T_m}{C_m+T_m},\mu=\frac{C_m-T_m}{2\left(C_m+T_m\right)}\right) \tag{8}$$

where $\tau_{\max}$ represents the maximum shear stress in polymer under certain loading conditions; I_1 is the first stress invariant; S_m, T_m and C_m are the shear strength, tensile strength and compressive strength of the matrix respectively.

The failure of the interphase is assumed to occur if one of the interfacial maximum stresses exceeds the corresponding allowable stress, which can be expressed as

$$\max\left\{\frac{<T_n^i>}{T_n^0},\frac{T_t^i}{T_t^0},\frac{T_s^i}{T_s^0}\right\}=1 \tag{9}$$

in which < > stand for the Macaulay brackets, which return the argument if positive and zero otherwise, so that there will be no damage when the interphase is under compression. T_n^i, T_t^i and T_s^i represent the interfacial normal, tangential and longitudinal shear traction respectively (Fig.2 (c)). T_n^0, T_t^0 and T_s^0 denote the interfacial normal, tangential and longitudinal shear strength respectively. The interfacial normal strength T_n^0 and the interfacial shear strength T_s^0 was considered as the unknown parameter during the whole analytical procedure of TFBT and 45FBT simulation.

During each increment of the macro FE model, the strain of each element integration point was read in the subroutine and acted as the overall strain of the GMC model. The micro stress and strain could be determined and employed for further damage analysis based on the failure criteria of the fiber, matrix and interphase. In the damage analysis, three field variables FV1, FV2 and FV3 were introduced to indicate the damage state of the fiber, interphase and matrix respectively. If one of the failure criteria was satisfied, the corresponding FV of the corresponding FE element increased from 0 to 1. The modulus decreased to a near zero value and the Poisson's ratio reduced to 0. The degraded properties were implemented for the next increment. The failure procedure would not stop until the damage spread all through the composite.

4 RESULTS AND DISCUSSION

4.1 Damage process

During the damage process, the fiber remained intact (FV1=0). The matrix only cracked (FV2=1) after the interfacial debonding occurred (FV3=1). The interfacial debonding was the dominated failure

mechanism for the damage of the T700S and T800H 45FBT specimens, which was consistent with experimental observation results. Figure 4 (a) and (b) shows the FV2 contour results during the tension process of the TFBT and 45FBT test with a weak interphase. In the composite layer, the red elements denote the failure regions while the intact regions are indicated with blue elements. The interfacial failure started at the free edge of the fiber bundle in TFBT specimens while the interfacial debonding in composite layer initiated at four antisymmetric corners which was adjacent to the matrix. Then the damage propagated with the increase of tensile displacement. Eventually the failure spread all through the whole bundle layer. Thus the multiscale failure model with reasonable parameters of interfacial strength is appropriate for simulating the damage process of the TFBT and 45FBT tests.

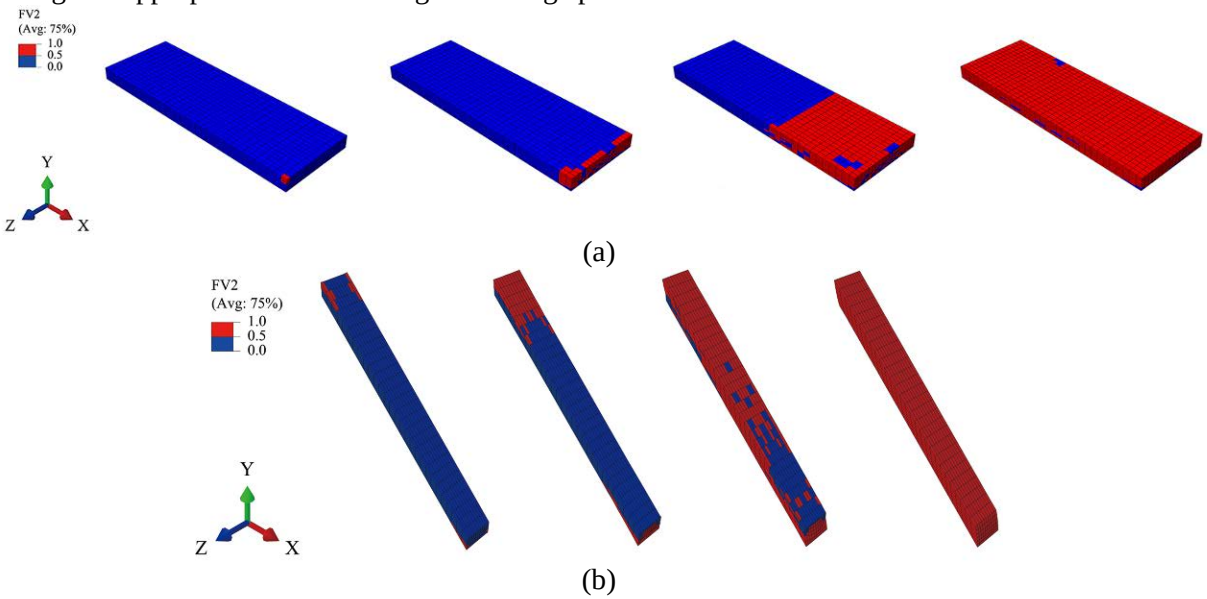

Figure 4: Damage process of the TFBT (a) and 45FBT (b) macro FE model

4.2 Interfacial stress

Figure 5 (a) plots the interfacial normal stress and tangential stress of the representative element at the free edge as a function of the circumferential coordinate θ for T700S/epoxy TFBT specimen. After thermal cooling, the interphase was under compression in the normal direction. When the following mechanical step was over, the state of stress varied from compression to tension. T_n^i at failure initiation was maximum at θ=0° which corresponded with the transverse loading direction. The maximum interfacial tangential stress was about one third of the maximum interfacial normal stress. So T_n^i rather than T_t^i is the dominated interfacial stress component which determines the interfacial damage of the representative element.

Three components of microscopic interfacial stresses of the firstly failed element in 45FBT sample were also plotted as a function of circumferential coordinate θ in Figure 5 (b). $T_{n,ther}^i$, $T_{t,ther}^i$ and $T_{s,ther}^i$ represent the interfacial thermal residual stress in the normal, tangential and longitudinal directions respectively. The interphase was compressed after cooling due to the macro compressive strain in ***2*** and ***3*** directions. The interfacial tangential and shear stresses were slightly lower than the interfacial normal stress. However, when the tensile step was over, the interfacial shear stress was much higher than the other two interfacial stresses. The interfacial shear stress was maximum at θ=90°. Though the interfacial normal stress became positive around θ=90°, the interphase was mostly compressed due to large compressive strain in ***2*** direction. The interfacial shear stress was the dominated interfacial stress component and induced the interphase to debond longitudinally, which could explain why interfacial shear strength T_s^0 was the most significant parameter in determining the failure initiation of 45FBT samples.

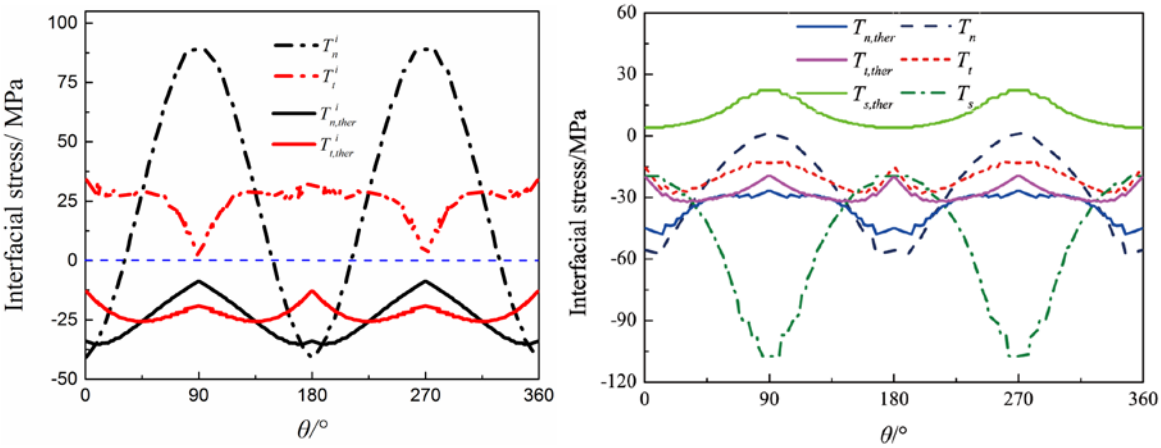

(a) (b)

Figure 5: Interfacial stress distribution in the TFBT (a) and 45FBT (b) specimen

4.3 Determination of interfacial strength

The precise value of interfacial shear strength was adjusted until the experimental and predicted values of 45FBT strength were equivalent. The results for TFBT samples as well as the corresponding 45FBT specimens were summarized in Table 1. All calculated ISS and INS values were based on the data of average tensile strength of the fiber bundle composite. It should be noted that the ISS of T800H/epoxy is 8.0 MPa higher than that of T700S/epoxy while the discrepancy of 45FBT tensile strength between these two material systems is only about 1.6 MPa. Since the multiscale model can give realistic results on the micro interfacial states, the calculated ISS rather than 45FBT tensile strength should be implemented for more accurate assessment of interfacial shear properties in the 45FBT test. Moreover, the 45FBT specimens can sustain more load than the TFBT samples. Both the macro tensile strength and calculated interfacial strength of 45FBT specimen are higher than TFBT samples, which was mainly caused by different loading conditions. For the carbon fiber/epoxy used in this work, the calculated interfacial normal strength accounts for approximately 84% of interfacial shear strength.

Fiber	σ_{TFBT}/MPa	σ_{45FBT}/MPa	INS/MPa	ISS/MPa
T700S	27.2±3.7	46.8±5.3	89.4	107.5
T800H	35.2±4.6	48.4±4.5	96.6	114.1

Table 1: A summary of experimental and analytical results

5 CONCLUSIONS

The TFBT and 45FBT tests were implemented based on the fiber bundle specimens to assess the interfacial normal strength (INS) and interfacial shear strength (ISS) of carbon fiber/epoxy system. The multiscale model consisting macro FE model and GMC micromechanics model considering the interphase was established to calculate the micro stress. And the TFBT test was found very sensitive to the IFNS while the IFSS dominated the failure of 45FBT samples. The TFBT and 45FBT tests with the corresponding multiscale model can be used to quantitatively evaluate the normal strength in the transverse direction and shear strength in the longitudinal direction of carbon fiber/epoxy interface. The calculated INS and ISS rather than tensile strength of fiber bundle specimens should be used for more accurate evaluation of fiber/matrix bonding strength.

ACKNOWLEDGEMENTS

This work was supported by Defense Industrial Technology Development Program of China (Grant No. A0520131001) and Natural Science Foundation of China (Grant No. 11572021).

REFERENCES

[1] S. Zhandarov, E. Mäder. Characterization of fiber/matrix interface strength: applicability of different tests, approaches and parameters. *Composites Science and Technology*, **65**, 2009, pp.149-160 (doi: 10.1016/j.compscitech.2004.07.003).

[1] E.U. Okoroafor, R. Hill. Determination of fibre-resin interface strength in fibre-reinforced plastics using the acoustic emission technique. *Journal of Physics D: Applied Physics*, **28**, 1995, pp. 1816-1825 (iopscience.iop.org/0022-3727/28/9/010).

[2] C. Ageorges, K. Friedrich, L. Ye. Experiments to relate carbon-fibre surface treatments to composite mechanical properties. *Composites Science and Technology*, **59**, 1999, pp. 2101-2113 (doi: 10.1016/S0266-3538(99)00067-6).

[3] Pindera M-J, Bednarcyk BA. An efficient implementation of the generalized method of cells for unidirectional, multi-phased composites with complex microstructures. *Composites Part B: Engineering*, **30**, 1999, pp. 87-105 (doi: 10.1016/S1359-8368(98)00040-7).

[4] G. Qi, S. Du, B. Zhang, Z. Tang, Y. Yu. Evaluation of carbon fiber/epoxy interfacial strength in transverse fiber bundle composite: Experiment and multiscale failure modeling. *Composites Science and Technology*, **105**, 2014,pp.1-8 (doi: 10.1016/j.compscitech.2014.09.014).

[5] G. Qi, S. Du, B. Zhang, Y. Yu. A new approach to assessing carbon fiber/epoxy interfacial shear strength by tensile test of 45° fiber bundle composites: Experiment, modeling and applicability. *Composites Science and Technology*, **129**, 2016, pp. 214-221(doi: 10.1016/j.compscitech.2016.04.032).